2011 IEEE International Conference on Robotics and Automation
Shanghai International Conference Center
May 9-13, 2011, Shanghai, China

An Adaptive Data Driven Model for Characterizing Rock Properties from Drilling Data

Hang Zhou, Peter Hatherly, Fabio Ramos and Eric Nettleton
Australian Centre for Field Robotics, The University of Sydney, Australia
{h.zhou, p.hatherly, f.ramos, e.nettleton}@acfr.usyd.edu.au

Abstract— **Autonomous operation of blast hole drill rigs requires monitoring of drilling parameters known as "Measurement While Drilling" (MWD) data. From these data, rock properties can be inferred. A supervised classification scheme is usually used to map MWD data inputs to rock type outputs given some labeled training data. However, the geology has no definite ground truth that can allow a reliable labeling of the training data, nor is there a clear input-output pair connection between the MWD data and the rock types. In this paper, an adaptive unsupervised approach is proposed to estimate the rock types in a data driven way by minimizing the entropy gradient of the characterizing measure - "Optimized Adjusted Penetration Rate" (OAPR). Neither data labeling nor fixed model parameters are required because of the data driven nature of the algorithm. Experimental results illustrate the effectiveness of our solution.**

I. INTRODUCTION

One of the world's major mining companies, Rio Tinto, is currently working to automate the operation of a large open pit iron ore mine in the Pilbara region of Western Australia. A significant challenge in this work is to build representations of the unmined (in-ground) geology to determine the location of the ore boundaries and the variations in the quality of the ore and host rocks. Identifying rock types plays an important role in numerous aspects of mining, e.g., rock boundary maps are useful for mine design and rock strength information can assist with the design of blasting patterns as well as the selection of drilling parameters.

Conventionally, geological modeling is accomplished manually by geologists using data from exploratory drilling. This process is time intensive and expensive on several accounts. Firstly, drilling and the logging of cores and chips takes time and is costly. Also, the subsequent geological modeling with the assistance of 3D software tools, is time consuming and strongly relies on geologists' experience and skills. In addition, models are constrained by rock boundaries, the locations of which may not be adequately known and also may not reflect real world situations where the changes in geology are gradual. All of these reasons motivate the development of a more efficient and precise solution.

For some time, blast hole drills have been equipped with drill monitors which record a drill's performance via measurements of mechanical performance settings such as penetration rate (PR), pulldown pressure (PP), rotation pressure (RP), rotation speed (RS) and bit air pressure (BAP), etc. These measurements are collectively known as "Measurement While Drilling" (MWD) data. In the case of the commonly used rotary drilling method, it is found that PR, PP and RP are the measurements that are most responsive to changing geological conditions.

(a) Autonomous blast hole drill rig used for collecting MWD data.

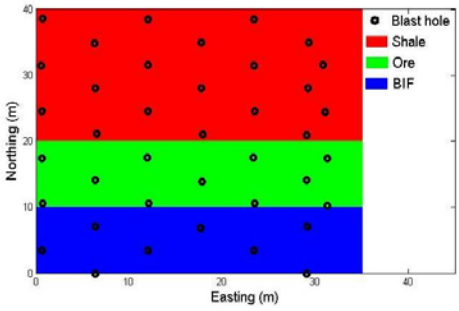

(b) Illustration of blast holes layout.

Fig. 1. Autonomous drill rig and the (partial) pattern of holes used to fragment needs prior to the mining of ore (the size of a typical mining bench is 30-40m wide by more than 200m long).

An autonomous blast hole drill rig used for collecting MWD data is shown in Figure 1(a). Figure 1(b) is a simplified illustration of a blast hole layout across major rock types of interest, which are typically shale, ore and banded iron formation (BIF). MWD data are collected from those blast holes which are typically 12m deep. In principle, variations in MWD data reflect changes in the physical properties of

978-1-61284-385-8/11/$26.00 ©2011 IEEE

the rocks and can provide direct evidence of the geological situation. For our work on developing an autonomous mine, machine learning techniques can therefore be used with these data to provide suitable geological interpretations, i.e., to build a function that maps the input MWD data to the output rock properties and to verify the results with an estimate of the ground truth provided by other means. Such a solution allows real time estimation of the types of rocks being drilled. For verification purposes, the ground truth needs to be estimated from the alternative data sources (such as drill chip assays from exploration and blast holes) that are used for conventional manual geological modeling. However, what makes this problem different to a typical machine learning problem is that there is not a clear one to one correspondence between the MWD values and the rock types. Any individual rock type can have a range of MWD representations. Also, prior to mining, absolute certainty about the geology and ground truth is not possible. Certainty after mining is also difficult to establish on account of the fragmentation of the rocks and the physical displacement that occurs as a result of blasting.

In response to these challenges, we adaptively transform the MWD data features into one single feature we call "Optimized Adjusted Penetration Rate" (OAPR). OAPR is expressed in a parameterized combination of PR, PP and RP as shown in eqn (1) so that the variation of the data can be better approximated. The function parameters θ_1 and θ_2 are estimated by minimization of the OAPR entropy gradient [3][4],

$$OAPR = f(PR, PP, RP, \theta_1, \theta_2), \tag{1}$$

where θ_1 and θ_2 are the function parameters.

As opposed to the existing entropy minimization solutions [6][7][8] which seek the absolute minimum entropy value, our parameter optimization minimizes the entropy gradient so that the targeted multi-modal pattern is easily identified. Gaussian Process regression [1] is then applied to the OAPR values of individual holes to create a more dense rock strength distribution.

The main contributions of this paper are:

1) On the application side, a novel flexible rock strength characterizing scheme has been proposed that categorizes the underlying pattern in a fully data driven way.
2) From the algorithm point of view, a new feature extraction method has been developed for adaptively deriving features out of the given data that effectively represents the underlying pattern, regardless of the data distribution and the number of categories.
3) As a key part of the proposed approach, parameter optimization of extracted features is distinctively carried out by entropy gradient minimization, which better reflects the intrinsic properties of the given data.

The remainder of this paper is organized as follows. Related work is briefly introduced in Section II. Section III describes the adaptive data modeling method. Section IV presents results of our approach on a mining site dataset. Finally, Section V summarizes the main conclusions.

II. Related Work

The idea of relating drilling measurements to the properties of rocks (i.e., the rock recognition problem) has been studied before in an empirical or statistical way [12][10][11][15][14], where Teale's Specific Energy of Drilling (SED) [12] is most widely cited. Machine learning techniques have also been applied to drilling data based rock recognition, including unsupervised learning [13] and supervised learning, such as Neural Networks (NN) [16][18][17][9], Conditional Random Field modelling [19][20] and Gaussian Process classification [21]. The supervised learning rock recognition methods classify rock types based on a model trained from the existing labeled datasets. The major problem of such a supervised learning approach is that, as mentioned above, accurate geological labeling for training the MWD data is difficult. Local and more gerneral variations in the geology create a situation where the ground truth of an unmined site is never precisely known.

As a precursor to our current approach, we have investigated means of identifying rock types by means of estimating the continuous rock strength distribution followed by a further clustering to rock types. In [22], a hybrid classification approach is presented by combining Gaussian Process regression with unsupervised clustering. An integrated MWD measure - "Adjusted Penetration Rate" (APR) is defined to convert the challenging classification problem to tractable regression and unsupervised clustering problems. At any point, APR is given by the penetration rate (PR) divided by the product of pulldown pressure (PP) and the square root of rotation pressure (RP), i.e.,

$$APR = PR/(PP * RP^{0.5}). \tag{2}$$

APR removes some of the variability in PR measurements caused by variations in PP and RP. It gives a good indication of rock strength which in turn bears a relationship to rock type. In general terms, for the three major rock types we are concerned with, shale is the weakest, followed by ore and BIF is the strongest.

However, the geology can vary significantly within a mine and between mines. The relationship between the drilling mechanics and the underlying rock characteristics is also not yet well explored and modeled. Therefore, it may not always be appropriate to use a single definition for APR. Further work is needed to extract the rock characterizing measure in a more stable and robust way.

III. Adaptive Rock Strength Modeling

As indicated in Section I, entropy is employed in our proposed approach to optimize the estimation of the rock strength measure - OAPR. Entropy, entropy gradient as well as relative entropy are briefly introduced in Section III-A. Section III-B describes the details of adaptive rock strength modeling.

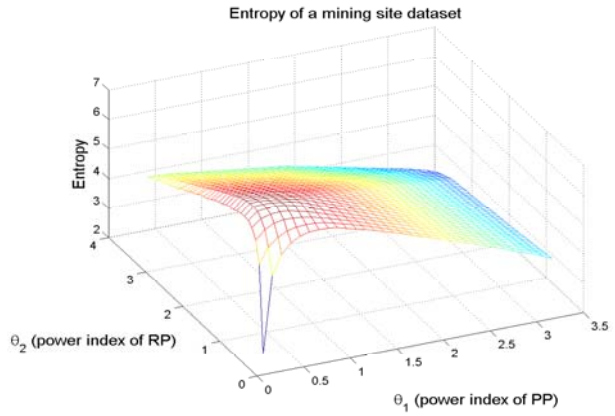

Fig. 2. Entropy distribution when altering θ_1 and θ_2 which are the power indices of PP and RP for a mining site dataset.

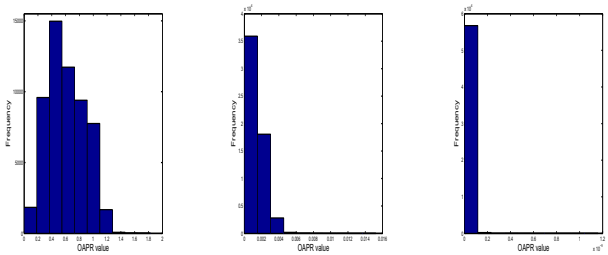

(a) θ_1=0.5 and θ_2=0.5. (b) θ_1=1.5 and θ_2=1.5. (c) θ_1=3.0 and θ_2=3.0.

Fig. 3. Changing of OAPR data distribution with θ_1 and θ_2 for the mining site dataset in Fig 2.

A. Entropy, Entropy Gradient and Relative Entropy

Entropy is a measure of the uncertainty which qualifies the information contained in a message with a given probability distribution [5].

Given a discrete random variable X with alphabet A and a probability mass function $p(x) = P(X = x)$, the entropy of X can be expressed as [5],

$$H(X) = -\sum_{x \in A} p(x) \log p(x). \tag{3}$$

For a real function of two variables $f(X, Y)$, the entropy of $f(X, Y)$ is,

$$H(f(X,Y)) = -\sum_{x,y \in A} p(f(x,y)) \log p(f(x,y)). \tag{4}$$

The entropy gradient, which is the differential change of entropy along the direction of largest directional derivative, is defined as,

$$\nabla H = \frac{\partial H}{\partial f} \cdot \frac{\partial f}{\partial x}\vec{\mathbf{x}} + \frac{\partial H}{\partial f} \cdot \frac{\partial f}{\partial y}\vec{\mathbf{y}}, \tag{5}$$

where $\frac{\partial H}{\partial f}$ is the partial derivative of H, $\frac{\partial f}{\partial x}$ and $\frac{\partial f}{\partial y}$ are the partial derivatives of f.

The magnitude of the entropy gradient is,

$$\begin{aligned} |\nabla H| &= |\frac{\partial H}{\partial f} \cdot \frac{\partial f}{\partial x}\vec{\mathbf{x}} + \frac{\partial H}{\partial f} \cdot \frac{\partial f}{\partial y}\vec{\mathbf{y}}| \\ &= \sqrt{(\frac{\partial H}{\partial f} \cdot \frac{\partial f}{\partial x})^2 + (\frac{\partial H}{\partial f} \cdot \frac{\partial f}{\partial y})^2}. \end{aligned} \tag{6}$$

To quantitatively compare the similarity between two distributions $q(x)$ and $r(x)$ (as done in Section IV), the Kullback-Leibler divergence (KL divergence, also called the relative entropy), is defined as follows, which can be taken as the "distance" between the two distributions,

$$D(q\|r) = -\sum_{x \in A} q(x) \log \frac{q(x)}{r(x)}. \tag{7}$$

B. Adaptive Rock Strength Modeling

As indicated in [22], it is very difficult for supervised learning to predict rock types from MWD data in a satisfactory way as the training data cannot be properly labeled due to the big uncertainty of the geology. A rock strength characterizing measure APR (as shown in eqn (2)) has been developed. Such an approximation does build the mapping between MWD data and rock strength, which is not explicitly shown on the raw data. However, due to the complexity of the underlying drilling mechanics and the geological variation from site to site, it is unlikely that such an approximation can consistently guarantee the satisfactory performance at various mining sites. On the other hand, explicitly building a more precise mapping between the MWD data and the rock strength is difficult as a definite model of the underlying drilling mechanics is unavailable.

Basically, APR can be taken as a feature extracted from the relevant MWD data features (PR, PP and RP). In general, feature extraction [2] constructs the combination of the given data features and transforms to a reduced feature set, so as to have a more efficient and accurate description of the data.

With regards to all the challenges mentioned above, we aim at extracting a new rock strength characterizing measure - called "Optimized Adjusted Penetration Rate" (OAPR) in an adaptive and fully data driven way, regardless of the underlying drilling mechanics and the variable geology. As a result of studying on the drilling operations, some simple rules are summarized (verified by the drilling experts and geologists) and used as the basic physical meaning assumptions in further feature extraction,

1) PP and RP are the major applied forces on changing PR, with joint impact in a factorized way. The impact of either PP and RP will not exceed $PP^{3.5}$ or $PP^{3.5}$ respectively.
2) PR is proportional to the rock strength with fixed PP and RP values.
3) Realistically, PP and RP are all subject to change in a correlated way, which also brings about changes on the PR value when drilling rocks of similar strength.
4) There exists a distribution of up to three major rock types (i.e., shale, ore and BIF). The rock strength is normally smooth within each rock type.

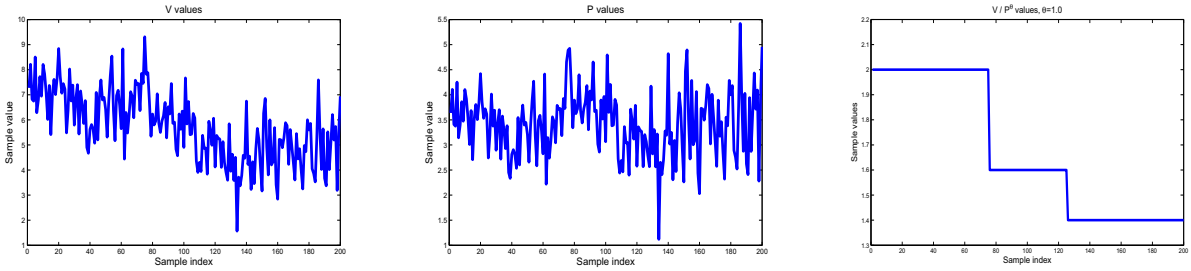

(a) Synthetic data dividend V. (b) Synthetic data divisor P. (c) Synthetic data quotient V / P^{θ}, $\theta = 1.0$.

Fig. 4. A synthetic example illustrating the convergence of the data quotient.

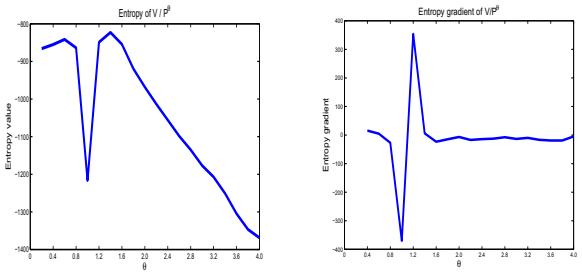

(a) Entropy of synthetic data quotient V / P^{θ}. (b) Entropy gradient of synthetic data quotient V / P^{θ}.

Fig. 5. Entropy and entropy gradient of the synthetic example.

Putting the above assumptions into consideration, we model OAPR as PR divided by a factorized combination of PP and RP. Since it is difficult to estimate the proportion of PP and RP that contribute to the correction of PR, we define OAPR in a flexible parameterized way as in eqn (8), i.e., PR is divided by the product of PP and RP to a power index of θ_1 and θ_2 respectively. θ_1 and θ_2 are the OAPR parameters.

$$OAPR(\theta_1, \theta_2) = PR/(PP^{\theta_1} * RP^{\theta_2}), \tag{8}$$

where $\theta_1 \in [0\ \ 3.5]$ and $\theta_2 \in [0\ \ 3.5]$ (assumption 1).

With OAPR being the rock strength characterizing measure, there exist the optimized parameter values $[\theta_1^*, \theta_2^*]$ that allow OAPR(θ_1^*, θ_2^*) to converge to and best match with the rock strength distribution (there could exist multiple optima which is beyond the scope of this paper). While for the rest of the $[\theta_1, \theta_2]$ values, OAPR(θ_1, θ_2) shows a less consistency with the existing rock strength distribution.

The optimized OAPR parameters $[\theta_1^*,\ \theta_2^*]$ are estimated through entropy analysis. As shown in eqn (8), OAPR is the function of two variables $[\theta_1,\ \theta_2]$, i.e., OAPR=$\phi(\theta_1, \theta_2)$. The probability distribution of OAPR is estimated on a n bins histogram. OAPR entropy is then calculated based on the derived histogram,

$$H(\phi(\theta_1, \theta_2)) = -\sum_{i=1}^{n} p(\phi_i(\theta_1, \theta_2)) \log p(\phi_i(\theta_1, \theta_2)), \tag{9}$$

where $\phi_i(\theta_1, \theta_2)$ is the number of $\phi(\theta_1, \theta_2)$ values dropped in the ith bin of the histogram, $p(\phi_i(\theta_1, \theta_2))$ is the percentage of $\phi(\theta_1, \theta_2)$ values dropped in the ith bin.

It should be noted that the conventional entropy minimization methods [6][7] do not apply to our case. As can be seen from eqn (8) that continuous increase of $[\theta_1,\ \theta_2]$ will monotonically decrease entropy towards creating a uniform distribution of OAPR and make the underlying rock strength converge to one class, which diverts from the expected three rock types in our application.

Figure 2 and Figure 3 show some intuitive illustrations of how entropy minimization works on OAPR. In Figure 2, OAPR entropy values decrease monotonically with the increasing of PP power index θ_1 and RP power index θ_2. Correspondingly, OAPR histogram plottings in Figure 3 show that the variety of OAPR values drop significantly with the increasing of θ_1 and θ_2. Obviously, absolute minimization of entropy will lead to a "flattened" data distribution, resulting in the unitary class, which is not what we try to reveal.

What is needed here is a method that can locate the optimized OAPR parameters $[\theta_1^*, \theta_2^*]$ properly w.r.t. to the three rock types. As indicated above, the optimized OAPR(θ_1^*, θ_2^*) distribution should be discriminative from the rest of the OAPR(θ_1, θ_2) distributions, and is supposed to better match with the rock strength distribution. Our tests on various datasets have shown that a sharp drop of the OAPR entropy gradient is strongly correlated to an optimized OAPR$[\theta_1, \theta_2]$ distribution that better approximates the rock type distribution.

This sharp entropy gradient change is a good reflection of the physical meaning assumptions in Section III-B. Any $[\theta_1, \theta_2]$ values other than the optimum $[\theta_1^*, \theta_2^*]$ will deviate the OAPR$[\theta_1, \theta_2]$ distribution from the three rock types approximation. This will greatly diversify the OAPR values, resulting in a much higher entropy value (and hence a high entropy gradient change). Essentially, OAPR optimum OAPR$[\theta_1^*, \theta_2^*]$) can be taken as the "anomaly" hidden in the non-optimum diversified OAPR values. It is indicated in [3] [4] that it is the entropy gradient not the entropy itself, that is correlated to the anomaly detection.

A simplified 1D illustration of how the entropy gradient varies with the changing of the power index of the divisor is shown in Figure 4 through to Figure 6 using 1D synthetic data. To simulate the typical three rock types that normally exist, we make the data in Figure 4(c) (which is the quotient of data in Figure 4(a) and Figure 4(b)) to have three

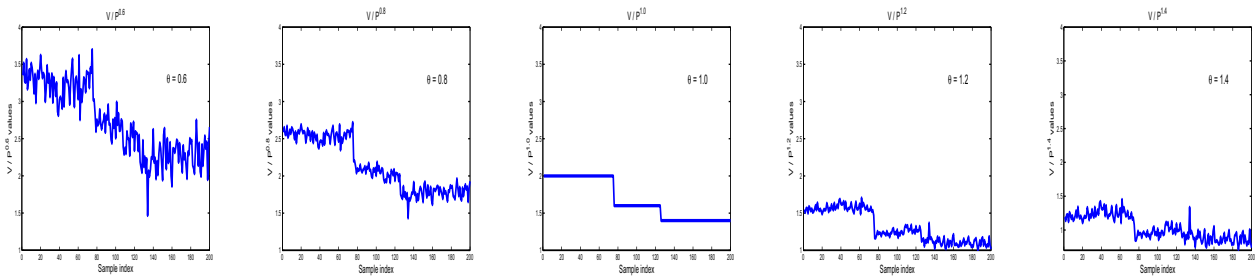

(a) Synthetic data quotient with $\theta = 0.6$. (b) Synthetic data quotient with $\theta = 0.8$. (c) Synthetic data quotient with $\theta = 1.0$. (d) Synthetic data quotient with $\theta = 1.2$. (e) Synthetic data quotient with $\theta = 1.4$.

Fig. 6. A synthetic example with varied parameters.

categories, which are assumed to be the underlying patterns.

Figure 5(a) and Figure 5(b) show the changes in entropy as well as the entropy gradient of the quotient V/P^{θ} w.r.t. the increasing of θ (this is a simplified version of simulating $PR/(PP^{\theta_1} * RP^{\theta_2})$ w.r.t. the increasing of θ_1 and θ_2 in eqn (8)). It can be seen that around the underlying pattern (where $\theta = 1$), the entropy gradient reaches its minimum. Figure 6(a) to Figure 6(e) plot the quotient V/P^{θ} versus θ, where the most distinguishable pattern (Figure 6(c)) appears at $\theta = 1$ when the corresponding entropy gradient reaches its minimum as in Figure 5(b).

Eqn (10) is the OAPR object function which seeks to optimize $[\theta_1, \theta_2]$ and minimize the gradient of the OAPR entropy,

$$[\theta_1^*, \theta_2^*] = \arg\min_{\theta_1,\theta_2}(sign(dH) \cdot |\nabla H(\phi(\theta_1, \theta_2))|), \quad (10)$$

where $|\nabla H(\phi(\theta_1, \theta_2))|$ is the gradient magnitude of the OAPR entropy w.r.t. θ_1 and θ_2, $sign(dH)$ is the sign of differential of H, θ_1^* and θ_2^* are the optimized values of θ_1 and θ_2 respectively.

IV. Experimental Results

Experiments have been carried out on the same mining data as those used in [22], which contains a good mixture of the three major rock types - shale, ore and BIF. Figure 7 shows a surface map with the locations of the blast holes as well as the assumed approximate rock type boundaries (the "ground truth"). The blast holes are 5-6m apart and 12m deep. The "ground truth" was provided by experienced geologists using alternative geological data, such as visual examination of drill chips, chemical assays and geophysical logging data. It is a reasonable approximation of the "ground truth".

The red zone represents shale, the weakest rock present (as discussed in Section I), the blue represents BIF which is the strongest and the green indicates ore which has intermediate strength. In the following results, the redder colors correspond to higher OAPR values which imply lower rock strength (likely to be shale), and the more blue colors indicate lower OAPR values corresponding to rocks with higher strength (likely to be BIF). Green colors represent the medium strength rocks (likely to be ore).

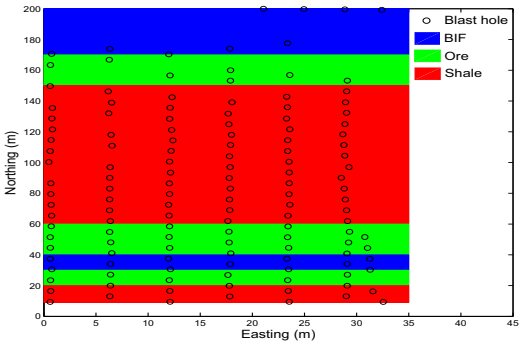

Fig. 7. Blast holes as well as the assumed rock type boundary "ground truth" of the experimental real mining site data.

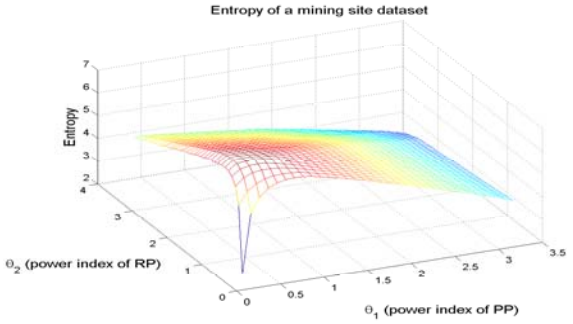

(a) Entropy of the real mining site data.

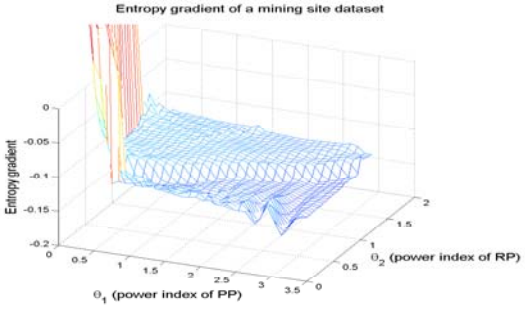

(b) Entropy gradient of the real mining site data.

Fig. 8. Entropy and entropy gradient of the real mining site data.

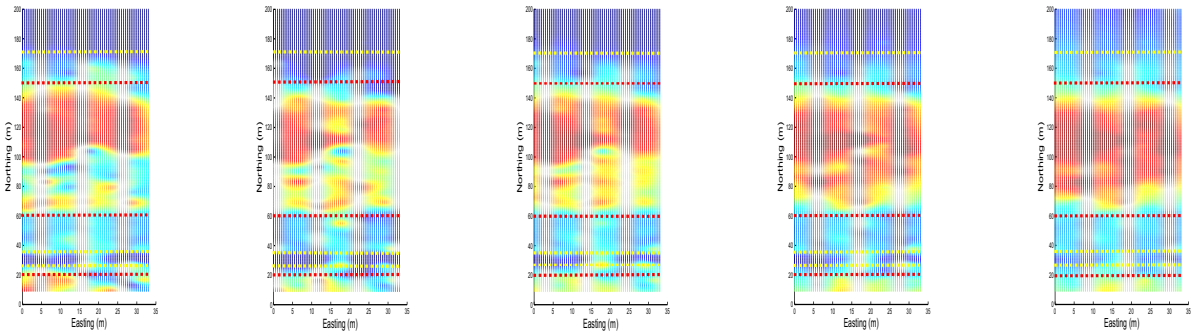

(a) Raw PR with $\theta_1 = 0$ and $\theta_2 = 0$. (b) OAPR with $\theta_1 = 0.5$ and $\theta_2 = 1.0$. (c) APR with $\theta_1 = 1.0$ and $\theta_2 = 0.5$. (d) OAPR with $\theta_1 = 2.0$ and $\theta_2 = 0.5$. (e) OAPR with $\theta_1 = 3.0$ and $\theta_2 = 0.0$.

Fig. 9. Rock strength from different PR/APR/OAPR values. Red dashed lines are the assumed shale/ore boundary, yellow dashed lines are the assumed ore/BIF boundary.

As described in Section III, OAPR values determined with varied values of θ_1 and θ_2 in the range [0, 3.5] are first calculated using eqn (8). This is a reasonable range because if values of θ go much beyond the upper bound 3.5, OAPR (eqn (8)) begins to loose the ability to discriminate between rocks other than the very soft and the very hard and the targeted tri-model pattern is lost.

Entropies as well as entropy gradients of the OAPR values are then calculated following eqn (9), eqn (5) and eqn (6) with the results shown in Figure 8(a) and Figure 8(b) respectively. For the entropy gradient in Figure 8(b), the minimum entropy gradient point and corresponding optimized $[\theta_1^*, \theta_2^*]$ parameters occur at $\theta_1^* = 3.0$ and $\theta_2^* = 0$. The extracted $[\theta_1^*, \theta_2^*]$ values are then fed into eqn (8) to derive the OAPR(θ_1^*, θ_2^*) values. GP regression on a more dense grid (0.5m apart) is further applied to the OAPR(θ_1^*, θ_2^*) values to get the distribution of rock strength shown in Figure 9. Here, the red dashed lines represent the assumed shale/ore boundaries and the yellow dashed lines for the assumed ore/BIF boundaries from the "ground truth".

Figure 9(a) and Figure 9(c) show results from [22] where Figure 9(a) is the rock strength distribution using the original PR. Figure 9(c) is the rock strength distribution using APR with $\theta_1 = 1.0$ and $\theta_2 = 0.5$. Figure 9(e) is the rock strength distribution using OAPR with θ_1 and θ_2 optimized by our proposed approach, i.e., $\theta_1 = 3$ and $\theta_2 = 0$. Compared with the geology in Figure 7 (which is used as the "ground truth"), Figure 9(e) is the best, with well established shale zones (red) and a distinct ore (green) and BIF (blue) zones.

To explore the changing trend of OAPR characteristics with θ_1 and θ_2, two more rock strength distributions are added in Figure 9(b) ($\theta_1 = 0.5$ and $\theta_2 = 1.0$) and Figure 9(d) ($\theta_1 = 2.0$ and $\theta_2 = 0.5$). As can be seen from Figure 8(b), in addition to the lowest entropy gradient value point, which is $\theta_1 = 3$ and $\theta_2 = 0$, there exists another major drop in the entropy gradient values along the diagonal direction of the θ_1 and θ_2 axes. $\theta_1 = 0.5$ and $\theta_2 = 1.0$ is on the upper left side of this major gradient drop with higher entropy gradient value, while $\theta_1 = 2.0$ and $\theta_2 = 0.5$ is located on the opposite side with a lower entropy gradient value.

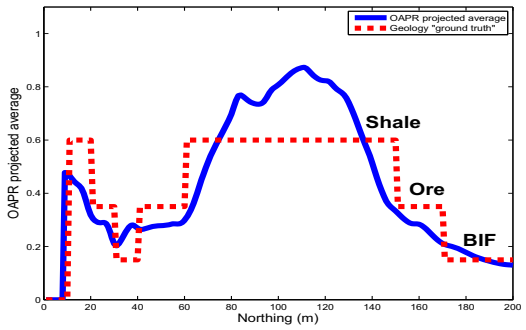

Fig. 10. 1D projected OAPR values with $\theta_1 = 3.0$, $\theta_2 = 0$ and the 1D projected "ground truth".

For all the results in Figure 9, the identification of the rock type zones gets consistently better from left to right, while the corresponding entropy gradient values in Figure 8(b) monotonically decrease. This shows that the entropy gradient is a key factor in allowing the OAPR to converge to the underlying rock patterns.

TABLE I

KULLBACK-LEIBLER DIVERGENCE COMPARISON ON DIFFERENT OAPR VAULES WITH VARIED REFERENCE GEOLOGY PARAMETERS.

KL_1 - KL DIVERGENCE W.R.T. BIF=0.15, ORE=0.35, SHALE=0.60,
KL_2 - KL DIVERGENCE W.R.T. BIF=0.30, ORE=0.40, SHALE=0.50,
KL_3 - KL DIVERGENCE W.R.T. BIF=0.10, ORE=0.50, SHALE=1.00

θ_1	θ_2	KL_1	KL_2	KL_3
0	0	69.38	71.57	4.23
0.5	1.0	52.05	54.15	-8.04
1.0	0.5	42.12	46.10	-17.08
2.0	0.5	17.34	22.33	-34.77
3.0	**0**	**8.26**	**15.19**	**-41.96**

The comparison of the results needs to be conducted visually because the "ground truth" for the geology of an unmined site is never precisely known (see Section II).

Qualitative judgement should be directed towards choosing solutions where the rock variations have relatively smooth and simple surfaces, and there is relatively little structure within each rock type.

To assess the performance of the OAPR characterized rock strength distribution in a more quantitative way, OAPR values in Figure 9 are projected to 1D on the "Northing" axis. The blue solid curve in Figure 10 is the 1D projection result of the OAPR values in Figure 9(e). The reference "ground truth" is also set up as the 1D projection result of the "ground truth" in Figure 7.

To compare the similarity between the 1D projection of OAPR and rock type "ground truth", the KL divergence is calculated following eqn (7). However, it should be noted that the two distributions $q(x)$ and $r(x)$ are taken as the spatial 1D distribution shown in Figure 10 rather than the probability distribution as it was originally defined in eqn (7), since the rock strength distribution is spatially oriented and concerned.

Table I lists the KL divergence results of OAPR values in Figure 9 w.r.t. three groups of reference "ground truth". With varied "ground truth" parameters, the KL divergence monotonically decreases along the five groups of OAPR values in Figure 9. The minimum KL divergence value occurs at $\theta_1 = 3.0$ and $\theta_2 = 0.0$. This quantitative examination is consistent with the visual examination of Figure 9 which suggests that that OAPR ($\theta_1 = 3.0, \theta_2 = 0.0$) best reflects the underlying rock structure. It is therefore inferred that the OAPR provides a robust method for distinguishing the rock types from drilling data.

V. Conclusions

A novel self adaptive scheme we have called the optimized adjusted penetration rate has been proposed for rock type categorization which minimizes the entropy gradient of the MWD based rock strength measure. Key advantages of this scheme are that prior data labeling is not needed and the model parameters can be adaptively estimated, guaranteeing a constant optimized modeling for all data. Experiments on actual data have shown that our proposed method has a satisfactory performance in identification of rock types.

VI. Acknowledgments

This work has been supported by the Rio Tinto Centre for Mine Automation and the ARC Centre of Excellence programme, funded by the Australian Research Council (ARC) and the New South Wales State Government. The authors also acknowledge the input from Annette Pal, Danielle Robinson, Florian Oppolzer of Rio Tinto, as well as Sildomar Monteiro and Ross Hennessy of Rio Tinto Centre for Mine Automation.

References

[1] Rasmussen, C.E., Williams, C.K.I.: Gaussian Processes for Machine Learning. The MIT Press, Cambridge, Massachusetts (2006).

[2] Ding, S., Jia, W., Su, C., Jin, F., Shi, Z.: A Survey on Statistical Pattern Feature Extraction. Proceedings of the 4th International Conference on Intelligent Computing: Advanced Intelligent Computing Theories and Applications - with Aspects of Artificial Intelligence, vol. 5227, pp. 701-708 (2008).

[3] May, E.C., James, S., Spottiswoode, P., James, C.L.: Shannon Entropy: A Possible Intrinsic Target Property. Journal of Parapsychology, vol. 58, pp. 384-401 (1994).

[4] May, E.C., James, S., Spottiswoode, P., Faith, L.V.: The Correlation of the Gradient of Shannon Entropy and Anomalous Cognition: Toward an AC Sensory System. Journal of Scientific Exploration, vol. 14(1), pp. 53-72 (2000).

[5] Gray, R.M.: Entropy and Information Theory. Springer-Verlag (1990).

[6] Brand, M.E.: Pattern Discovery via Entropy Minimization. Unvertainty 99: International Workshop on Artificial Intelligence and Statistics (1999).

[7] Donoho, D.L., Chui, C.K., Montefusco, L., Puccio, L.: On Minimum Entropy Segmentation. Wavelets: Theory, Algorithms, and Applications, pp. 233-269 (1994).

[8] Meger, D., Gupta A., Little, J.J.: Viewpoint Detection Models for Sequential Embodied Object Category Recognition. In Proceedings of International Conference on Robotics and Automation (2010).

[9] Gonzalez, J. E. J. M.: Application of Pattern Recognition Techniques to Monitoring-While-Drilling on a Rotary Electric Blasthole Drill at an Open-Pit Coal Mine. Thesis for Master of Science (2007).

[10] Scoble, M. J., Peck, J.: A Technique for Ground Characterization Using Automated Production Drill Monitoring. International Journal of Mining, Reclamation and Environment, vol. 1(1), pp. 41-54 (1987).

[11] Scoble, M. J., Peck, J., Hendricks, C.: Correlation between Rotary Drill Performance Parameters and Borehole Geophysical Logging. Mining Science and Technology, vol. 8, pp. 301-312 (1989).

[12] Teale, R.: The Concept of Specific Energy in Rock Drilling. International Journal of Rock Mechanics and Mining Sciences, vol. 2, pp. 57-73 (1965).

[13] King, R. L., Hicks, M. A. Signer, S. P.: Using Unsupervised Learning for Feature Detection in a Coal Mine Roof. Engineering Applications of Artificial Intelligence, vol. 6, pp. 565-573 (1993).

[14] Schunnesson, H.: Rock Characterisation Using Percussive Drilling. International Journal of Rock Mechanics and Mining Sciences, vol. 35(6), pp. 711-725 (1998).

[15] Finfinger, G. L., Wilson, G., Peng, S., Thomas, B., Gu, Q.: An Approach to Identifying Geological Properties from Roof Bolter Drilling Parameters. Conference on Ground Control in Mining (2000).

[16] Utt, W. K.: Neural Network Technology for Strata Strength Characterization. International Joint Conference on Neural Networks (1999).

[17] Finfinger, G. L.: A Methodology for Determining the Character of Mine Roof Rocks. PhD Thesis (2003).

[18] Labelle, D., Bares, J., Nourbakhsh, I.: Material Classification by Drilling. 17th International Symposium on Automation and Robotics in Construction (2000).

[19] Monteiro, S., Ramos, F., Hatherly, P.: Learning CRF Models from Drill Rig Sensors for Autonomous Mining. NIPS workshop: Learning from Multiple Sources with Applications to Robotics (2009).

[20] Monteiro, S., Ramos, F., Hatherly, P.: Conditional Random Fields for Rock Characterization Using Drill Measurements. International Conference on Machine Learning and Applications (2009).

[21] Zhou, H., Monteiro, S., Hatherly, P., Ramos, F., Oppolzer,F., Nettleton, E.: Spectral Feature Selection for Automated Rock Recognition Using Gaussian Process Classification. In Proceedings of Australian Conference on Robotics and Automation (2009).

[22] Zhou, H., Hatherly, P., Monteiro, S., Ramos, F., Oppolzer, F., Nettleton, E.: A Hybrid GP Regression and Clustering Approach for Characterizing Rock Properties from Drilling Data. Technical Report ACFR-TR-2011-001 http://www.acfr.usyd.edu.au/techreports/index.php (2010).